

Functional renormalization group for nonequilibrium quantum many-body problems

R. Gezzi, Th. Pruschke, and V. Meden
 Institut für Theoretische Physik, Universität Göttingen,
 Friedrich-Hund-Platz 1, D-37077 Göttingen, Germany
 (Dated: April 15, 2024)

We extend the concept of the functional renormalization for quantum many-body problems to nonequilibrium situations. Using a suitable generating functional based on the Keldysh approach, we derive a system of coupled differential equations for the m -particle vertex functions. The approach is completely general and allows calculations for both stationary and time-dependent situations. As a specific example we study the stationary state transport through a quantum dot with local Coulomb correlations at finite bias voltage employing two different truncation schemes for the infinite hierarchy of equations arising in the functional renormalization group scheme.

PACS numbers: 71.27.+a, 73.21.La, 73.23.-b

I. INTRODUCTION

The reliable calculation of physical properties of interacting quantum mechanical systems presents a formidable task. Typically, one has to cope with the interplay of different energy-scales possibly covering several orders of magnitude even for simple situations. Approximate tools like perturbation theory, but even numerically exact techniques can usually handle only a restricted window of energy scales and are furthermore limited in their applicability by the approximations involved or the computational resources available. In addition, due to the divergence of certain classes of Feynman diagrams, some of the interesting many-particle problems cannot be tackled by straight forward perturbation theory.

The situation becomes even more involved if one is interested in properties of equilibrium, in particular time-dependent situations. A standard approach for such cases is based on the Keldysh formalism¹ for the time evolution of Green functions, resulting in a matrix structure of propagators and self-energies. This structure is a direct consequence of the fact that in nonequilibrium we have to calculate averages of operators taken not with respect to the ground state but with respect to an arbitrary state. Therefore, the Gell-Mann and Low theorem² is not valid anymore. Other approaches attempt to treat the time evolution of the nonequilibrium system numerically, for example using the density matrix renormalization group³, the numerical renormalization group (NRG)^{4,5} or the Hamiltonian based flow-equation method.⁶

The Keldysh technique shows a big flexibility and one therefore can find a wide range of applications such as transport through atomic, molecular and nano devices under various conditions,⁷ systems of atoms interacting with a radiation field in contact with a bath,^{8,9} or electron-electron interaction in a weakly ionized plasma.¹⁰

One powerful concept to study interacting many-particle systems is the rather general idea of the renormalization group¹¹ (RG), which has also been applied to time-dependent and stationary nonequilibrium situations recently.^{12,13,14,15,16} In the RG approach one usu-

ally starts from high energy scales, leaving out possible infrared divergences and works ones way down to the desired low-energy region in a systematic way. However, the precise definition of "systematic way" does in general depend on the problem studied.

In order to resolve this ambiguity for interacting quantum mechanical many-particle systems in equilibrium, two different schemes attempting a unique, problem independent prescription have emerged during the past decade. One is Wegner's Hamiltonian based flow-equation technique,^{17,18} the second a field theoretical approach, which we want to focus on in the following. This approach is based on a functional representation of the partition function of the system and has become known as functional renormalization group (fRG).^{19,20,21,22}

A detailed description of the various possible implementations of the fRG and its previous applications in equilibrium can be found e.g. in Refs. 23 and 24. In the present work we extend the fRG to nonequilibrium by formulating the problem on the real instead of the imaginary time axis using the functional integral representation of the action on the Keldysh contour. Within a diagrammatic approach a similar set of fRG flow equations has already been derived by Jakobs and Schoeller and applied to study nonlinear transport through one-dimensional correlated electron systems.^{25,26} We believe that this method will enable us to treat a variety of nonequilibrium problems within a scheme which is well established in equilibrium and in contrast to other approaches is comparatively modest with respect to the computer resources required. Our framework for nonequilibrium will turn out to be sufficiently general to allow for a treatment of systems disturbed by arbitrary external fields (bias voltage, laser field, etc.), which can be constant or time-dependent.

For classical many-body problems the fRG (also called nonperturbative renormalization group) was used to study nonequilibrium transitions between stationary states.²⁷

As a simple but nontrivial application to test the potential and weakness of our implementation of a nonequilibrium fRG we choose the single impurity Anderson

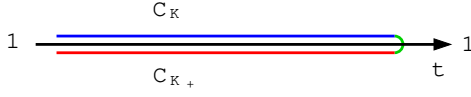


FIG. 1: (color online) Keldysh contour

model (SIAM).²⁸ This model represents the paradigm for correlation effects in condensed matter physics and is at the heart of a large range of experimental^{29,30,31,32,33,34,35} and theoretical investigations.^{36,37} It furthermore is the standard model for the description of the transport properties of interacting single-level quantum dots.

The paper is organized as follows. In Sec. II and the appendices we extend the equilibrium fRG to treat general nonequilibrium quantum many-body problems. As an example we study the finite bias, stationary transport through an Anderson impurity in Sec. III. Within the nonequilibrium extension we obtain a system of coupled tensor equations, which represent the flow of the different components (in the Keldysh space) of the self-energy and the vertex function. We discuss two approximations derived from the fRG scheme that have been successfully applied to the equilibrium situation.^{38,39} A summary and outlook in Sec. IV concludes the paper.

II. FUNCTIONAL RG IN NONEQUILIBRIUM

We start from the standard definition of the two-time Green function

$$G(\vec{0};) = i\hbar S^{-1} \Gamma(\vec{0}) \gamma(\vec{0}) S; \quad (1)$$

in the interaction picture, where Γ comprises a set of single-particle quantum numbers and time t . The time evolution operators are given as

$$S = T \exp \left[-i \int_1^9 V_I(t) dt \right]; \quad (2)$$

$$S^{-1} = \bar{T} \exp \left[i \int_1^9 V_I(t) dt \right]; \quad (3)$$

with T the usual time ordering and \bar{T} the anti time-ordering operator. The interaction term $V_I(t)$ is arbitrary, including possible explicit time dependence.

In a nonequilibrium situation, the propagation of the system from $1 \rightarrow 1$ is not any more equivalent to the propagation from $1 \rightarrow 1$, i.e. one has to distinguish whether the time arguments in Eq. (1) belong to the former or latter.^{40,41,42} This scheme is usually depicted by the Keldysh double-time contour shown in Fig. 1, where C_K represents the propagation $1 \rightarrow 1$ (upper branch of the Keldysh contour) and C_{K+} the propagation $1 \rightarrow 1$ (lower branch of the Keldysh contour). Consequently, one has to introduce four distinct propagators, namely the time-ordered Green function

$$G(\vec{0};) = i\hbar T \Gamma(\vec{0}) \gamma(\vec{0}) i \\ = i \langle \bar{\psi}(t) \psi(t) \rangle = i \langle \psi(t) \bar{\psi}(t) \rangle; \quad (4)$$

where $t, t' \in C_K$, the anti time-ordered Green function

$$G^{++}(\vec{0};) = i\hbar \bar{T} \Gamma(\vec{0}) \gamma(\vec{0}) i \\ = i \langle \psi(t) \bar{\psi}(t') \rangle = i \langle \bar{\psi}(t') \psi(t) \rangle; \quad (5)$$

with $t, t' \in C_{K+}$ and

$$G^+(\vec{0};) = i\hbar \Gamma(\vec{0}) \gamma(\vec{0}) i; t \in C_{K+}; t' \in C_K \quad (6) \\ G^-(\vec{0};) = i\hbar \gamma(\vec{0}) \Gamma(\vec{0}) i; t \in C_K; t' \in C_{K+} \quad (7)$$

where $\gamma = +1$ for bosons and $\gamma = -1$ for fermions. Concerning the Keldysh indices we here follow the notation of Ref. 40. $G(\vec{0};)$ and $G^{++}(\vec{0};)$ take into account the excitation spectrum while $G^+(\vec{0};)$ and $G^-(\vec{0};)$ describe the thermodynamic state of the system. Only three of the Green functions are independent and one commonly introduces the linear combinations

$$G^R(\vec{0};) = (t - t') G^+(\vec{0};) + G^-(\vec{0};) \quad (8)$$

$$G^A(\vec{0};) = (t - t') G^-(\vec{0};) + G^+(\vec{0};) \quad (9)$$

$$G^K(\vec{0};) = G^+(\vec{0};) + G^-(\vec{0};); \quad (10)$$

named retarded, advanced and Keldysh component, respectively.

To derive a nonequilibrium fRG scheme for an interacting many-body problem along the lines of Refs. 23 and 24 one needs a formulation that allows to express the many-particle vertices as functional derivatives of a generating functional. Here we use the approach by Kamenev.⁴³ To set up a functional integral representation of the generating functional we define the matrix

$$\hat{G} = \begin{pmatrix} G & G^+ \\ G^+ & G^{++} \end{pmatrix}$$

and the short hand notation

$$\hat{O} = i \int_1^9 d\vec{0} \langle \hat{\chi}(\vec{0}); \gamma(\vec{0}) \rangle;$$

where

$$\hat{\chi} = \begin{pmatrix} \chi \\ \chi^+ \end{pmatrix}$$

is a spinor of fields (Grassmann for fermions or complex for bosons) with χ having a time from the upper branch of the Keldysh contour and χ^+ a time from the lower. Later it will also prove useful to Fourier transform from time t to frequency ω . One then has to replace t in χ by ω . The integrals over $\vec{0}$ and γ stand for summations over the quantum numbers and integrations over time or frequency. The following steps can be performed with either containing time or frequency. The generalization of the functional integral representation of the partition function to nonequilibrium is⁴³

$$= \frac{1}{0} \int_0^Z D \exp \left[i \int_0^Z \hat{G}_0^{-1} (f g; f g) + i S_{\text{int}}(f g; f g) \right] ; \quad (11)$$

The matrix \hat{G}_0 denotes the propagator of the noninteracting part of the many-body problem and S_{int} is the (arbitrary) interaction term.

To construct a generating functional for m -particle Green functions, one introduces external source fields and

$$W(f g; f g) = \frac{1}{0} \int_0^Z D \exp \left[i \int_0^Z \hat{G}_0^{-1} (f g; f g) + i S_{\text{int}}(f g; f g) \right] ; \quad (12)$$

The (connected) m -particle Green function $G_m^{(c)}$ can then be obtained by taking functional derivatives

$$G_m^{(c)}(f g; f g) = (i)^m \frac{\delta^m}{\delta f_1 \dots \delta f_m} \frac{\delta^m}{\delta g_1 \dots \delta g_m} W^{(c)}(f g; f g) \quad (13)$$

with

$$W^{(c)}(f g; f g) = \ln [W(f g; f g)] ; \quad (14)$$

The derivatives in Eq. (13) are taken with respect to the spinors f and g , i.e. the resulting Green function $G_m^{(c)}$ is a tensor of rank $2m$ in the Keldysh indices. In the following we adopt the notation that quantities with explicit index m are tensors of rank $2m$; without index m we denote the propagator and self-energy, both carrying a hat to point out their matrix structure.

Introducing the fields

$$f = i \frac{\delta}{\delta g} W^{(c)}(f g; f g) ; \quad g = i \frac{\delta}{\delta f} W^{(c)}(f g; f g) \quad (15)$$

we can perform a Legendre transformation

$$f g; f g = W^{(c)}(f g; f g) + \int_0^Z \hat{G}_0^{-1} (f g; f g) ; \quad (16)$$

to the generating functional of the one-particle irreducible vertex functions Γ_m (tensors of rank $2m$ in the Keldysh indices)

$$\Gamma_m(f g; f g) = i^m \frac{\delta^m}{\delta f_1 \dots \delta f_m} \frac{\delta^m}{\delta g_1 \dots \delta g_m} f g; f g \quad (17)$$

In contrast to the usual definition⁴⁴ of Γ_m for convenience (see Appendix A) we added a term $\int_0^Z \hat{G}_0^{-1} (f g; f g)$ in Eq.

(16). The relations between the $G_m^{(c)}$ and Γ_m in imaginary time can be found in text books⁴⁴ and can straightforwardly be extended to real times on the Keldysh contour. For example, for the one-particle Green function one obtains

$$\begin{aligned} G_1(f g; f g) &= G_1^c(f g; f g) \\ &= i \frac{\delta}{\delta g} \frac{\delta}{\delta f} W^{(c)} = \hat{G}_0^{-1} ; \\ &= \int_0^Z \hat{G}_0^{-1} (f g; f g) ; \end{aligned}$$

where

$$\hat{G}_0^{-1} = \hat{G}_0^{-1} \hat{\Lambda}^{-1} ;$$

with the proper one-particle self-energy $\hat{\Lambda}$. This implies the relation $\hat{\Lambda} = \hat{G}_0^{-1}$. We have a matrix structure not only with respect to f and g (as in equilibrium), but also with respect to the Keldysh indices. How does this additional structure manifest itself in the Green functions (13)? For $m = 1$ we have two derivatives with respect to spinor fields, i.e. the structure of a tensor product, which can be made explicit by using a tensor product notation

$$G_1^c(f g; f g) = (i) \frac{\delta}{\delta g} \frac{\delta}{\delta f} W^{(c)} ;$$

leading to the matrix

$$G_1^c(\omega; \epsilon) = (i)^d \frac{\frac{2W^c}{(\omega)} + \frac{2W^c}{(\omega) + (\epsilon)}}{\frac{2W^c}{(\omega)} + \frac{2W^c}{(\omega) + (\epsilon)}} \quad (18)$$

Up to now we extended standard textbook manipulations⁴⁴ from imaginary time to the real-time Keldysh contour. We emphasize that no translational invariance in time is assumed. To derive the fRG flow equations in nonequilibrium we can follow the steps of Ref. 24. In Eqs. (11) and (12) we replace the noninteracting propagator by a propagator \hat{G}_0 depending on a parameter $\omega \in [0; \infty]$ and require

$$\hat{G}_0^< = 0; \quad \hat{G}_0^> = \hat{G}_0; \quad (19)$$

i.e. at the starting point $\omega = 0$ no degrees of freedom are "turned on" while at $\omega = \infty$ the free problem is recovered. In models with infrared divergences can be used to regularize the problem. In equilibrium this is often achieved by implementing as an infrared cutoff in momentum or energy. One of the advantages of the fRG approach over other RG schemes is that one is not restricted to these choices and other ways of introducing the parameter have turned out to be useful for equilibrium problems.^{45,46} All that is required to derive the fundamental flow equations (23) and (B1) (see below) are the conditions Eq. (19). In our application of the nonequilibrium fRG to the steady state transport through an interacting quantum dot it is natural to implement as an energy cutoff. However, such a choice must not be the natural one in cases where one is interested in studying transient behavior. In this situation the propagator and the vertex functions in general depend on several spatial and time variables and there is no obvious momentum or energy cutoff scheme. Within the fRG several ways of introducing can be worked out, compared and the one best suited for the problem under investigation can be identified.

Through \hat{G}_0 the quantities defined in Eqs. (11) to (17) acquire a ω -dependence. Taking the derivative with respect to ω one now derives a functional differential equation for Γ . From this, by expanding in powers of the external sources, an infinite hierarchy of coupled differential equations for the Γ_m is obtained. Although the steps in the derivation are formally equivalent to Ref. 24, because of the real-time formulation additional factors i and signs appear in several places. We thus believe that it is helpful to present the details of the derivation for the present approach, which is done in Appendix A.

In particular, for the flow of the self-energy one finds the expression

$$\frac{d}{d\omega} \Sigma_1(\omega; \epsilon) = \frac{d}{d\omega} \Sigma^<(\omega; \epsilon);$$

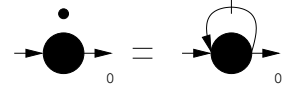


FIG. 2: Diagrammatic form of the flow equation for Σ_1 . The slashed line stands for the single scale propagator \hat{S} .

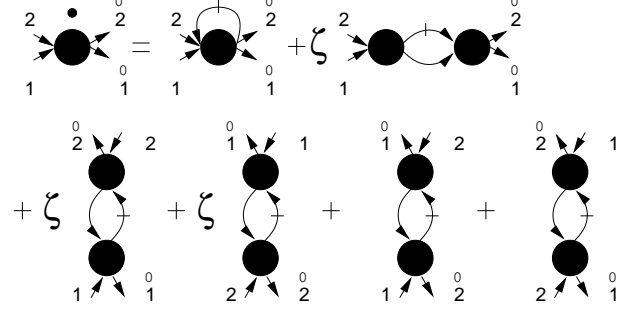


FIG. 3: Diagrammatic form of the flow equation for Γ_2 . The slashed line stands for the single scale propagator \hat{S} , the unslashed line for \hat{G} .

$$\frac{d}{d\omega} \Gamma_2(\omega; \epsilon; \epsilon; \epsilon) = \text{Tr} \left[\hat{S}^h \hat{G}_0^i \right] \quad (20)$$

which can be visualized by the diagram in Fig. 2. The trace in Eq. (20) is meant to run over all quantum numbers and time respectively frequency. In Eq. (20) appears the so-called single scale propagator (the slashed line in Fig. 2)

$$\hat{S} = \hat{G} \hat{Q} \hat{G}; \quad (21)$$

$$\hat{Q} = \frac{d}{d\omega} \hat{G}_0^h \hat{G}_0^i; \quad (22)$$

and the quantity $\Gamma_2(\omega; \epsilon; \epsilon; \epsilon)$ denotes the matrix obtained by keeping the indices ϵ and ω fixed.

We thus arrive at an expression that is formally identical to Eq. (19) in Ref. 24. The difference appears in the matrix structure, which now also contains the index components for the branches of the Keldysh contour. To make this explicit, we write out Eq. (20) with respect to the Keldysh structure

$$\frac{d}{d\omega} \Gamma_2^i = \text{Tr} \left[\hat{S}^h \hat{G}_0^i \right] \quad (23)$$

where ϵ and ω denote Keldysh indices and take the values \pm . Apparently, the derivative of Γ_1 is determined by Γ_1 and the two-particle vertex Γ_2 . Thus an equation for Γ_2 is required. The structure of this equation turns out to be similar to Eq. (21) of Ref. 24. Here we only show the diagrams representing it in Fig. 3, the full expression is given in Eq. (B1). The differential equation for Γ_2 does not only contain Γ_1 implicitly via the propagators \hat{G} and \hat{G}_0 , but also the three-particle vertex Γ_3 . The flow of the three-particle vertex depends on the four-particle vertex etc. It is generically possible to solve

the full set of infinitely many coupled differential equations. In applications one has to truncate it, and this is usually done at order $m = 2$, i.e. one replaces all vertices with $m > 2$ by their initial values, which for problems with a two-particle interaction means $\Gamma_m = \Gamma_m^0 = 0$ for $m > 2$. Even within this truncated system the remaining set of differential equations must typically further be approximated to allow for an analytical or a numerical solution.^{38,39,47} At the end of the RG flow, that is for $\Gamma_m^0 = 0$, the $\Gamma_m^0 = \Gamma_m$ present approximations to the many-body vertex functions from which observables can be computed (for examples see Sec. III).

We again note that a similar set of flow equations was derived by Jakobs and Schoeller using a diagrammatic approach.^{25,26}

III. APPLICATION TO QUANTUM DOTS

The derivation of the flow equations in the previous section and the appendices was completely general and they can be used to study time dependent or stationary properties of systems at finite temperature T or $T = 0$. A simple but nonetheless nontrivial application is nonequilibrium, stationary transport through an interacting single-level quantum dot at $T = 0$. For a stationary situation, time translational invariance holds and one can Fourier transform to frequency space. Moreover, because the quantum dot is a zero-dimensional structure, no additional degrees of freedom except spin have to be taken into account, thus considerably reducing the complexity of the problem.

Nonequilibrium theory of single-level quantum dots described by the SIAM (see below) has been a major subject of research over the past years. Several techniques have been developed respectively applied, for example statistical^{48,49,50}, perturbative,^{51,52,53,54,55,56,57,58,59,60} RG based^{13,15,16} and numerical procedures.^{5,6} In particular the RG based calculations were up to now restricted to situations away from the Kondo regime, either by looking at features in the mixed-valence state¹³ or in strong magnetic fields.^{15,16} Despite this tremendous ongoing effort, relatively little is known about nonequilibrium properties, even in the stationary state, of the model. On the other hand, the very detailed knowledge of the equilibrium properties⁶¹ makes it possible to interpret certain features or even discuss approximations on the basis of this fundamental understanding.

A. Single impurity Anderson model

The standard model to describe transport through interacting quantum dots is the SIAM.²⁸ Experimentally,^{29,62} the dot region is attached to two external leads, and the current is driven by an applied bias voltage V_B . Furthermore, the filling of the dot can be controlled by a gate voltage V_G . To keep the notation

simple we use units with $e = \hbar = 1$. The Hamiltonian reads

$$H = \sum_{\mathbf{k}, l} \epsilon_{\mathbf{k}, l} c_{\mathbf{k}, l}^\dagger c_{\mathbf{k}, l} + \sum_{\mathbf{k}, l} V_{\mathbf{k}, l} d^\dagger c_{\mathbf{k}, l} + U n_d + \sum_{\mathbf{k}, l} V_{\mathbf{k}, l} c_{\mathbf{k}, l}^\dagger d + H_{\text{sc}}. \quad (24)$$

in standard second quantized notation ($n = d^\dagger d$). As usual, \mathbf{k} is the wave vector of the band states in the leads and the spin. In addition, the index $l = L, R$ distinguishes the left and right reservoirs which can have different chemical potentials μ_l through an applied bias voltage $V_B = \mu_L - \mu_R$. Since we do not include a magnetic field lifting the spin-degeneracy of the spin up and down level, the one-particle Green function and the self-energy are spin independent and we suppress the spin index. We assume the dispersions $\epsilon_{\mathbf{k}, l}$ and hybridizations $V_{\mathbf{k}, l}$ between dot and the left and right leads to be identical, and $V_{\mathbf{k}} = V = \frac{1}{2}$ to be \mathbf{k} -independent. Equation (24) is written such that for $V_G = 0$ we have particle-hole symmetry.

The interaction in the Hamiltonian is reduced to the dot site only. We can thus reduce the problem to a zero-dimensional one by integrating out the leads. For the flow equations we need the propagator $\hat{G}_{d;0}$ at $U = 0$. To this end we use the Dyson equation to obtain^{1,40,42}

$$\hat{G}_{d;0}(\omega) = \frac{1}{0 - \omega + V_G} \hat{G}_{\text{lead}}^{-1}(\omega); \quad (25)$$

where

$$\hat{G}_{d;0} = \frac{1}{G_{d;0} + G_{d;0}^+}; \quad \hat{G}_{\text{lead}} = \frac{V^2}{2N} \sum_{\mathbf{k}, l} \frac{G_{\mathbf{k}, l} + G_{\mathbf{k}, l}^+}{G_{\mathbf{k}, l}^+ G_{\mathbf{k}, l}}; \quad (26)$$

To further evaluate Eq. (26), we have to insert the Green functions of the free electron gas, given by

$$G_{\mathbf{k}, l}(\omega) = \frac{1}{\omega - \epsilon_{\mathbf{k}, l} + i\eta} \quad (27)$$

$$+ 2i \frac{f(\epsilon_{\mathbf{k}, l})}{\hbar} \frac{1}{\omega - \epsilon_{\mathbf{k}, l} + i\eta};$$

$$G_{\mathbf{k}, l}^{++}(\omega) = G_{\mathbf{k}, l}(\omega); \quad (28)$$

$$G_{\mathbf{k}, l}^+(\omega) = 2i \frac{f(\epsilon_{\mathbf{k}, l})}{\hbar} \frac{1}{\omega - \epsilon_{\mathbf{k}, l} + i\eta}; \quad (29)$$

$$G_{\mathbf{k}, l}^-(\omega) = 2i \frac{f(\epsilon_{\mathbf{k}, l})}{\hbar} \frac{1}{\omega - \epsilon_{\mathbf{k}, l} + i\eta}; \quad (30)$$

into Eq. (25). This leads to

$$G_{d;0}(\omega) = \frac{1}{(\omega - V_G)^2 + \frac{1}{2} [f_L(\omega) + f_R(\omega)]}; \quad (31)$$

$$G_{d;0}^{++}(\omega) = [G_{d;0}(\omega)]^{-1}; \quad (32)$$

$$G_{d;0}^{+}(\omega) = i \frac{[f_L(\omega) + f_R(\omega)]}{(\omega - V_G)^2 + \gamma^2}; \quad (33)$$

$$G_{d;0}^{+}(\omega) = i \frac{[f_L(\omega) + f_R(\omega)]}{(\omega - V_G)^2 + \gamma^2}; \quad (34)$$

where $f_{1,2}(\omega) = f(\omega - \epsilon_{1,2})$ are the Fermi functions of

the leads and $\gamma = \pi \rho_F$, with ρ_F the density of states at the Fermi level of the semi-infinite leads, represents the tunnel barrier between the leads and the impurity.

Finally, the quantities we want to calculate are the current J through the dot and the differential conductance $G = dJ/dV_B$. For the model (24) the current is given by^{7,55}

$$J = \frac{1}{2} (J_L + J_R) = \frac{i}{2} \int d\omega [f_L(\omega) - f_R(\omega)] G_d^{+}(\omega) G_d^{+}(\omega); \quad (35)$$

where we already used that the left and right couplings are identical, i.e. $\Gamma_L = \Gamma_R = \gamma$, and summed over both spin directions. The interacting one-particle Green function of the dot is denoted by \hat{G}_d and $J_{L=R}$ are the currents across the left and right dot-lead contacts respectively. Equation (35) is written in a somewhat unusual form, not employing the relation $G_d^{+}(\omega) G_d^{+}(\omega) = G_d^R(\omega) G_d^A(\omega) = 2i\omega$, where ω denotes the dot's one-particle spectral function. The reason for this will be explained below.

Another quantity of interest is $J = J_L - J_R$.⁵² Obviously, since no charge is produced on the quantum dot, $J = 0$ in the exact solution. Using again the results of Refs. 7 and 55, the expression for J becomes

$$J = - \int d\omega \frac{F(\omega) [f_L(\omega) - f_R(\omega)]}{\omega} \quad (36)$$

$$\tilde{F}(\omega) = \omega - V_G + i \Gamma [f_L(\omega) - f_R(\omega)] \quad (37)$$

$$F(\omega) = f_L(\omega) + f_R(\omega) \quad (37)$$

where we used that $f_L(\omega)$ and $f_R(\omega)$ are purely imaginary. Depending on the type of approximation used $J = 0$ might either hold for all parameters^{55,60} or not.⁵² We note that fulfilling $J = 0$ is, however, not sufficient for an approximation to provide reliable results. E.g. the self-consistent Hartree-Fock approximation fulfills $J = 0$, but nonetheless does not capture the correct physics even in equilibrium.⁶¹

B. Lowest order approximation

Before studying the coupled system for \hat{S} and \hat{S}_2 we begin with the simpler case where we replace \hat{S}_2 on the right hand side of Eq. (23) by the antisymmetrized bare interaction and consider only the flow of \hat{S} . The only nonzero components of the bare two-particle vertex are those with all four Keldysh indices being the same ($=$)⁴⁰

$$\hat{S}_2^{(0)}(i_1 i_2; i_1 i_2) = iU \delta_{i_1 i_2} \delta_{i_1 i_2} \quad (38)$$

With this replacement Eq. (23) reduces to

$$\frac{d}{d\omega} \hat{S}^{(0)} = iU \frac{d}{d\omega} S^{(0)}(\omega) \quad (39)$$

Within this approximation the self-energy is always time or frequency independent, and no terms off-diagonal in the Keldysh contour indices are generated. It leads to at least qualitatively good results in equilibrium,³⁸ and has the additional advantage that the flow equations can be solved analytically.

As the last step we specify how the parameter ω is introduced. Since we are interested in a stationary situation, i.e. the propagators only depend on the time difference $t - t^0$, all equations can be transformed into frequency space and one natural choice is a frequency cutoff of the form

$$\hat{G}_{d;0}(\omega) = (\omega - i\gamma) \hat{G}_{d;0}(\omega) \quad (40)$$

with $\gamma = 1$.²⁴ Evaluating \hat{S} by means of the Morris lemma^{21,24} results in

$$\hat{S}^{(0)}(\omega) = (\omega - i\gamma) \frac{1}{\omega - i\gamma} \quad (41)$$

A straightforward calculation permits us thus to rewrite Eq. (39) as

$$\frac{d}{d} \quad ; \quad = \quad \frac{iU}{2} \quad X \quad \frac{G_{d;0}^{++}(\Gamma)}{(\Gamma)} \quad ; \quad \frac{G_{d;0}^{++}(\Gamma)}{(\Gamma)} \quad ; \quad \frac{G_{d;0}^{++}(\Gamma)G_{d;0}^{++}(\Gamma)}{(\Gamma)^2} \quad ; \quad (42)$$

where

$$\begin{aligned} (\Gamma) &= G_{d;0}^{++}(\Gamma)G_{d;0}^{++}(\Gamma) - G_{d;0}^{++}(\Gamma)G_{d;0}^{++}(\Gamma) \\ &= \frac{1}{(\Gamma - V_G)^2 + \frac{1}{2}} \end{aligned}$$

Finally, the initial condition for the self-energy is $\lim_{\Gamma \rightarrow 0} \chi_0 = 0$.²⁴

1. Equilibrium

We now focus on $T = 0$. In a first step we discuss the equilibrium situation, that is $V_B = V_L = V_R = 0$. Then we obtain the decoupled system

$$\frac{d}{d} \quad ; \quad = iU \frac{V_G}{[(\Gamma - i)^2 + (V_G - i)^2]} \quad ; \quad (43)$$

which can be solved analytically. We first note that with $++i = -i$ both equations are equivalent. For $-i$ we obtain with the definition $\Gamma = V_G + i$ the solution

$$\frac{i J_1\left(\frac{\Gamma}{U}\right) - (\Gamma + i) J_0\left(\frac{\Gamma}{U}\right)}{i Y_1\left(\frac{\Gamma}{U}\right) - (\Gamma + i) Y_0\left(\frac{\Gamma}{U}\right)} = \frac{J_0\left(\frac{V_G}{U}\right)}{Y_0\left(\frac{V_G}{U}\right)} \quad ; \quad (44)$$

where J_n and Y_n are the Bessel functions of first and second kind. The desired solution of the cutoff-free problem is obtained by setting $\Gamma = 0$, i.e.

$$\frac{J_1\left(\frac{\Gamma}{U}\right)}{Y_1\left(\frac{\Gamma}{U}\right)} - \frac{J_0\left(\frac{\Gamma}{U}\right)}{Y_0\left(\frac{\Gamma}{U}\right)} = \frac{J_0\left(\frac{V_G}{U}\right)}{Y_0\left(\frac{V_G}{U}\right)} \quad ; \quad (45)$$

which is precisely the result Eq. (4) obtained by Andergassen et al.³⁸ It is, however, important to note that in this work, based on the imaginary-time formulation of the fRG, the differential equation has a different structure. It is real and has a positive definite denominator. Thus, while the solutions at $\Gamma = 0$ are identical for the imaginary-time and real-time formulations, the flow towards $\Gamma = 0$ will show differences. As we will see next, the complex nature of the differential equation (43) can lead to problems connected to its analytical structure when attempting a numerical solution. For small $U = 1$ no particular problems arise. As an example the result for the flow of χ_0 as function of Γ for $U = 1$ and $V_G = 0.5$ obtained with a standard Runge-Kutta solver is shown in Fig. 4. Consistent with the analytical

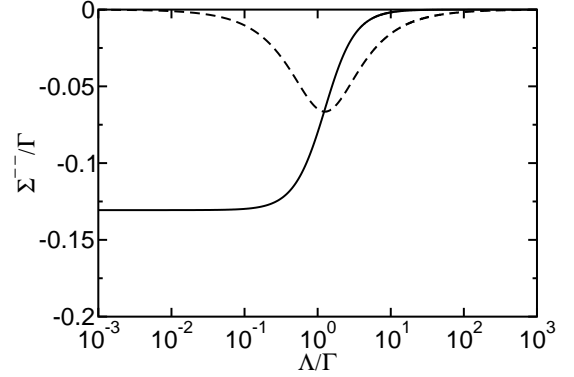


FIG. 4: Flow of $\chi_0 = \chi_0$ with $\Gamma = 0$ for $U = 1, V_G = 0.5$, and $V_B = 0$. The full curve shows the real part, the dashed the imaginary part of χ_0 .

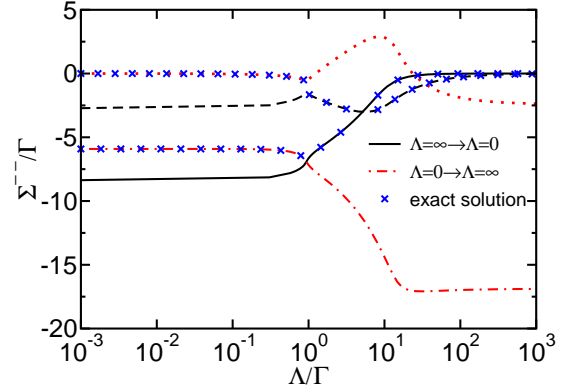


FIG. 5: (color online) Flow of $\chi_0 = \chi_0$ with $\Gamma = 0$ for $U = 15, V_G = 6$, and $V_B = 0$. The full and dashed curves show real and imaginary part obtained from the integration $\Gamma = 1 \rightarrow 0$, the dashed-dotted and dotted curves real and imaginary part obtained from an integration $\Gamma = 0 \rightarrow 1$, using the solution from (45) as initial value for χ_0 . The crosses denote the analytical solution (44).

solution Eq. (45), the imaginary part (dashed line) goes to zero as $\Gamma \rightarrow 0$, while the real part (solid line) rapidly approaches the value given by formula (45).

However, for larger values of U the numerical solution becomes unstable in a certain regime of V_G . A typical result in such a situation is shown in Fig. 5. The different curves were obtained as follows: The full and dashed ones from the numerical solution starting with $\chi_0 = 0$ at $\Gamma = 1$, the dash-dotted and dotted

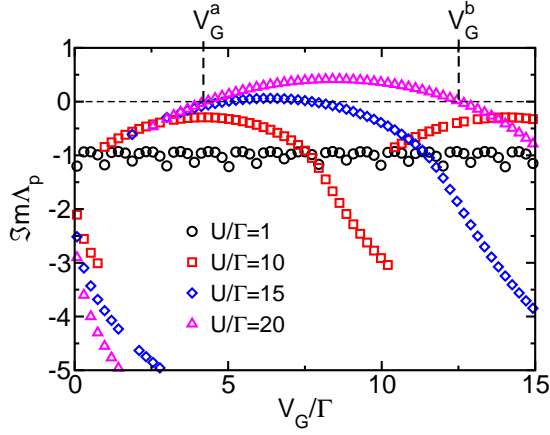


FIG. 6: (color online) Imaginary part of Λ_p determined from (44) and $V_G + i\epsilon = p + i$ for different values of U and $V_B = 0$ as function of V_G . For $U = 15$ and 20 there exist an interval $[V_G^a; V_G^b]$ where $\text{Im} \Lambda_p > 0$, while for small U or $V_G \notin [V_G^a; V_G^b]$ we always have $\text{Im} \Lambda_p < 0$.

by integrating the differential equation (43) backwards from $\epsilon = 0$ with the correct solution for $\epsilon = 0$ as given by formula (45) as initial value. The crosses really are the results from the analytical solution Eq. (44). Evidently, there exists a crossing of different branches of solutions to the differential equation for $\epsilon = 1$ and the numerical solution with starting point $\epsilon = 1$ picks the wrong one as $\epsilon \rightarrow 0$. The reason for this behavior is that for large U there exists a certain V_G^a such that $V_G + i\epsilon = p + i$ with real p , resulting in a pole in the differential equation (43). For $V_G \notin [V_G^a; V_G^b]$ this pole does not appear for real p , but as shown in Fig. 6 $\text{Im} \Lambda_p$ changes sign at V_G^a , which in turn induces a sign change on the right hand side of the differential equation, leading to the behavior observed in Fig. 5. There also exists a second critical value V_G^b such that for $V_G > V_G^b$ we find $\text{Im} \Lambda_p < 0$ and the instability has vanished again.

Obviously, this instability limits the applicability of the present approximation to sufficiently small values of U . This is different from the imaginary-time approach by Andergassen et al.,³⁸ where this simple approximation leads to qualitative correct results even for values of U significantly larger than Γ .

2. Nonequilibrium

We now turn to the case of finite bias voltage V_B . As a typical example, the flow of Γ for $U = 1$ (full and dashed curves) and 5 (dashed-dotted and dotted curves) for $V_G = 0.5$ at $V_B = 0$ (equilibrium) and $V_B = 1$ is shown in Fig. 7. Since the results for Γ^{++} are related to those for Γ by $\Gamma^{++} = \Gamma$ we do not show them here. The V_B dependence of the curves for $\epsilon = 1$ (thick lines) looks sensible. For $V_B \neq 0$ an

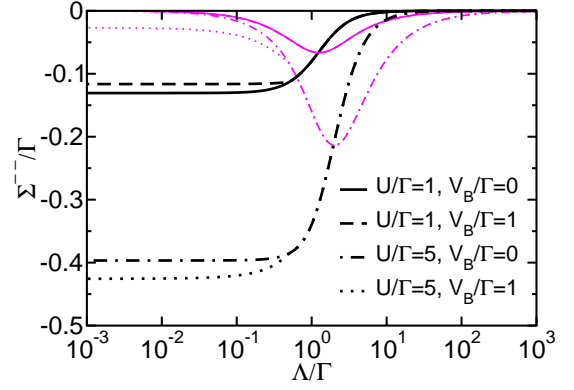


FIG. 7: (color online) Flow of Γ with $\Gamma = 0.5$ for $U = 1$ and 5 for $V_G = 0.5$ at $V_B = 0$ and 1 (thick curves: real part; thin curves: imaginary part). The curve for $\Gamma = 1$ at $U = 1$ and $V_B = 1$ (thin dashed line) lies on top of the corresponding zero bias curve and is thus not visible.

imaginary part of order U^2 is generated in the flow which does not vanish for $\epsilon \rightarrow 0$ (see the thin dotted line). Causality requires that the relation

$$(\Gamma) + \Gamma^{++}(\Gamma) = \Gamma^{++}(\Gamma) + \Gamma(\Gamma) \quad (46)$$

must hold for the exact solution. Because of $\Gamma^{++}(\Gamma) = \Gamma^{++}(\Gamma) = 0$, the finite imaginary part of Γ leads to a breaking of the condition (46) to order U^2 at the end of the RG flow. This is consistent with the fact that by neglecting the flow of the vertex terms of order U^2 are only partially kept in the present RG truncation scheme. To avoid any confusion we emphasize that our RG method is different from any low-order perturbation theory. The weak breaking of causality can also be understood as a consequence of our approximation leading to a complex, energy-independent self-energy: The off-diagonal components, being related to the distribution functions for electrons and holes, respectively, in general have different support on the energy axis. The energy independence makes it impossible to respect this structure here.

For our further discussion the order U^2 violation of Eq. (46) means that we may not rely on relations like Eqs. (8)-(10) but have to work with G , thus the somewhat unusual formula (35). A naive application of $G_R = G_d^{++}$ and use of $G_d^{++} = 2i\text{Im} G_d^R$ would have led to unphysical results. That working with $G_d^{++} = G_d^{++}$ is still sensible can be seen from a straightforward evaluation leading to

$$G_d^{++}(\Gamma) = G_d^{++}(\Gamma) = \quad (47)$$

$$2i \frac{\Gamma \Gamma_V + i \Gamma [F(\Gamma)]}{\Gamma^2 + 2F(\Gamma)F(\Gamma)}$$

$$F(\Gamma) = f_L(\Gamma) + f_R(\Gamma)$$

which is purely imaginary with a definite sign. Inserting the expression (47) into the formula (35), one can

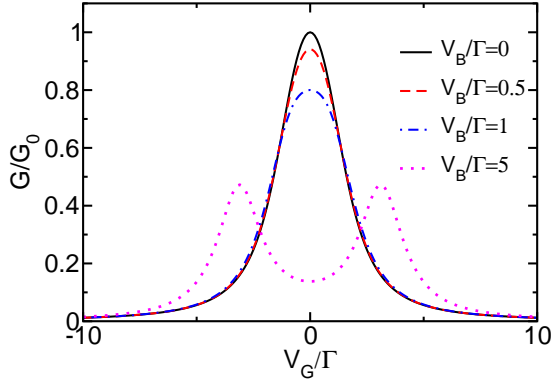


FIG. 8: (color online) Conductance normalized to $G_0 = 2e^2/h$ as function of V_G for $U = 2$ and several values of the bias voltage V_B .

calculate the current and thus the conductance. Since we are at $T = 0$, an explicit expression for the current of the cut-off problem (at $\omega = 0$) can be obtained by noting that with $V_L = V_B = 2$, $V_R = -V_B = -2$ one has $f_L(\omega) = f_R(\omega) = \theta(V_B - 2 - \omega)$ and $F(\omega) = 1$ for $|\omega| < 2$ [$V_B = 2; V_B = 2$], which leads to

$$J = \frac{2}{V_B} \int_{-V_B}^{V_B} d\omega \frac{1}{V_G + \omega^2} = \frac{2}{V_B} \int_{-V_B}^{V_B} d\omega \frac{1}{V_G + \omega^2} \quad (48)$$

$$= \frac{2}{V_B} \arctan \frac{V_G + \frac{V_B}{2}}{\omega} \Big|_{-V_B}^{V_B}$$

with the abbreviations

$$V_G = V_G + e \quad ; \quad (49)$$

$$= \frac{p}{2 + (em)^2} : \quad (50)$$

Equation (48) for the current is equivalent to the non-interacting expression but with renormalized parameters V_G and p , which depend on the interaction as well as the bias and gate voltage.

An example for the differential conductance as function of V_G obtained from Eq. (48) for $U = 2$ and several values of V_B is shown in Fig. 8, where $G_0 = 2e^2/h$ (after reintroducing e and h). Increasing V_B leads, as expected, first to a decrease of the conductance close to $V_G = 0$ and later to a splitting of order V_B . Since we will discuss a more refined scheme including parts of the flow of the two-particle vertex next, we do not intend to dwell too much on the results of this simplest approximation. We note in passing that for $V_G = 0$ due to particle-hole symmetry we obtain from the differential equation (42) that $J = 0$ independent of U . Consequently the current J calculated via Eq. (48) and the conductance are independent of U , too, and given by the corresponding expressions for the noninteracting system. As we will see in the next section, this deficiency will be cured by the

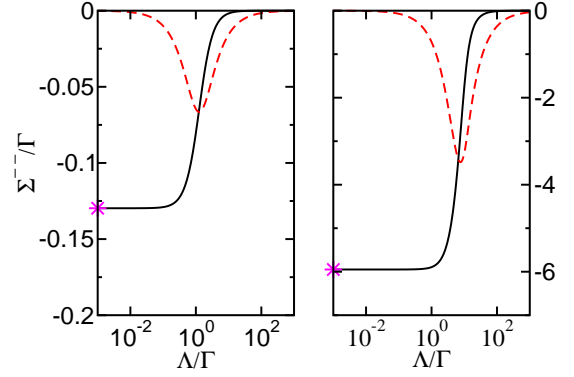


FIG. 9: (color online) Flow of $\Sigma' = \Sigma'(\omega)$ with $\omega = 0$ for $U = 1$ (left panel) and $U = 15$ (right panel) at $V_G = U = 2$ and $V_B = 0$. The full curves show the real part, the dashed the imaginary part of Σ' . The stars at the vertical axis denote the values as obtained from the imaginary-time FRG.³⁹

approximate inclusion of the vertex flow. In the present approximation the current conservation $J = 0$ holds for all parameters as $\Sigma' = \Sigma' = 0$ [cf. Eq. (36)].

C. Flowing vertex

A more refined approximation is obtained when we insert the flowing two-particle vertex γ_2 as given by expression (B2) in the calculation of the self-energy Eq. (23). By this we introduce an energy-dependence of the self-energy.²⁴ However, because the size of the resulting system of differential equations becomes extremely large if the full frequency dependence is kept (for a discussion on this in equilibrium see Ref. 24), we only keep the flow of the frequency independent part of the vertex, an additional approximation which has successfully been used in equilibrium.³⁹ As a consequence we again end up with a frequency independent $\hat{\gamma}$. The resulting expression for the self-energy (see Appendix B) is

$$\frac{d}{d\Lambda} \Sigma' = \frac{1}{2} \sum_{\omega} G_d(\omega) \gamma_2(\omega) 2U \gamma_2(\omega) U \gamma_2(\omega) ; \quad (51)$$

where $U \gamma_2$ is the flowing interaction given by the expression (B3). As has been observed by Karrasch et al.,³⁹ this approximation leads to a surprisingly accurate description of the transport properties in equilibrium. In particular it is superior to the lowest order approximation including only the bare vertex.

1. Equilibrium

We again begin with the discussion of the solution to Eq. (51) in equilibrium. Results for the flow of Σ' are presented in Fig. 9 for $U = 1$ (left panel) and $U = 15$

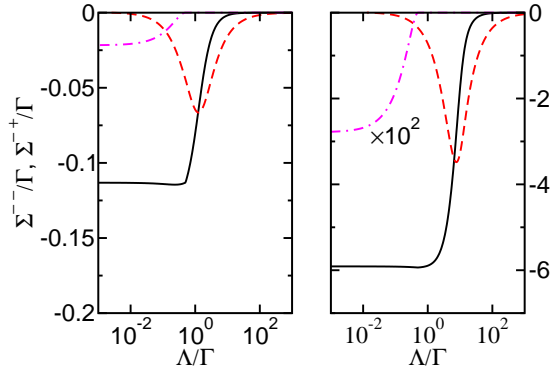


FIG. 10: (color online) Flow of Σ^-/Γ and Σ^+/Γ with $\Gamma = 1$ (left panel) and $U = 15$ (right panel), $V_G = U=2$ and $V_B = 1$. The full curves show the real part, the dashed the imaginary part of Σ^-/Γ , the dot-dashed the imaginary part of Σ^+/Γ . The real part for the latter is zero.

(right panel) for $V_G = U=2$. Since $\Sigma^+/\Gamma = 0$, only one component is shown. The stars in Fig. 9 denote the solutions of the imaginary-time equations taken from Ref. 39. Note that for $U = 15$ and $V_G > 6$ the simple approximation Eq. (42) showed an instability, while with the flowing vertex the system is stable even for these large values of U and reproduces the correct equilibrium solutions for $\beta \rightarrow 0$.³⁹ The reason for this is that the flow of the vertex reduces the resulting effective interaction below the critical value in the instability region.³⁹

2. Nonequilibrium

For the same parameters as in Fig. 9 we present the resulting flow with finite bias $V_B = 1$ in Fig. 10. In addition to the curves for real (solid lines) and imaginary

part (dashed lines) of Σ^-/Γ a third curve is displayed, the imaginary part of Σ^+/Γ (dashed-dotted lines), which now is generated during the flow. Note that $\langle e^{\pm i\epsilon} \rangle = 0$ and $\Sigma^+/\Gamma = \Sigma^-/\Gamma$. Furthermore, we always find $\text{Im} \Sigma^+/\Gamma < 0$. For $U = 15$ (right panel in Fig. 10) we have rescaled $\text{Im} \Sigma^+/\Gamma$ by a factor 10^2 to make it visible on the scale of $\text{Im} \Sigma^-/\Gamma$. Since Σ^-/Γ is a complex energy independent quantity Eq. (46) is again not fulfilled. We note that the error is still of order U^2 , but for fixed V_G and V_B it is significantly smaller than in the simplest truncation scheme discussed above.

The energy-independence of the self-energy allows to derive an analytical expression for the current at $T = 0$ similar to Eq. (48), which due to the appearance of Σ^+/Γ now becomes

$$J = -\frac{\tilde{X}}{s=1} \arctan \frac{V_G + s \frac{V_B}{2}}{\tilde{X}} \quad (52)$$

with V_G as in Eq. (49) and

$$\tilde{X} = \frac{\text{Im} \Sigma^+/\Gamma}{\tilde{X}^2 + (\text{Im} \Sigma^-/\Gamma)^2};$$

where \tilde{X} is taken at $\epsilon = 0$. Thus, the only change to the expression (48) is a formal replacement $\tilde{X} \rightarrow \tilde{X}$. Equation (52) is of the same structure as for the noninteracting case with V_G and \tilde{X} replaced by renormalized parameters. However, the two self-energy contributions Σ^-/Γ and Σ^+/Γ enter distinctively different in the expression for the current. While $\text{Im} \Sigma^-/\Gamma$ solely plays the role of an additional lifetime broadening, $\text{Im} \Sigma^+/\Gamma$ directly modifies the tunneling rate both in the prefactor of J and in the expression for the lifetime broadening.

A problem occurs when using the results of the present approximation in Eq. (36), leading to

$$J = 2 - \frac{d!}{1} \frac{\tilde{X}}{V_G + i [\text{Im} \Sigma^-/\Gamma]} \frac{\text{Im} \Sigma^+/\Gamma [\text{Im} \Sigma^-/\Gamma]}{J^2 + [\text{Im} \Sigma^-/\Gamma] + \text{Im} \Sigma^+/\Gamma [\text{Im} \Sigma^-/\Gamma]} : \quad (53)$$

The requirement $J = 0$ is only fulfilled for $V_G = 0$, because then $\tilde{X} = 0$ and the integrand is asymmetric with respect to ϵ . Thus our approximation of an energy-independent flowing vertex violates current conservation for $V_G \neq 0$ in nonequilibrium. We verified that $J \propto U^2$ which is consistent with the fact that not all terms of order U^2 are kept in our truncated RG procedure. How does J behave in the limit $V_B \rightarrow 0$? To see this we note that, because $\text{Im} \Sigma^+/\Gamma$ does not depend on the sign of V_B and furthermore goes to zero as $V_B \rightarrow 0$, $\text{Im} \Sigma^+/\Gamma \propto V_B \rightarrow 0$

V_B^2 . Consequently, $J \propto V_B \rightarrow 0$ and hence the violation of current conservation vanishes in the linear response regime $V_B \rightarrow 0$.

In Fig. 11 we show the current at $V_G = 0$ as function of V_B for $U = 1, 6$ and 15 . With increasing U the current for intermediate V_B is strongly suppressed. In addition there occurs a structure at low V_B , which turns into a region of negative differential conductance with increasing U . The appearance of such a shoulder in the current was observed in other calculations as well.^{51,52,56} However,

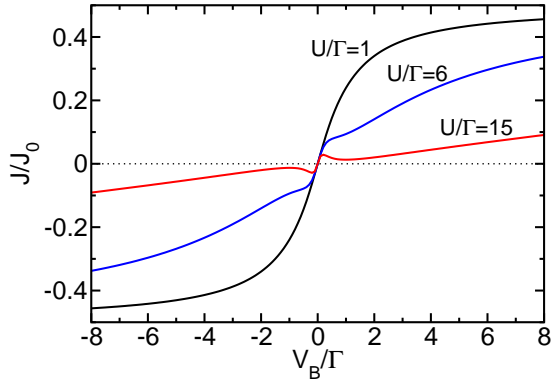


FIG. 11: (color online) Current normalized to $J_0 = G_0 \frac{e}{h}$ (after reintroducing e and h) as function of V_B for $U = 1, 6$ and 15 and $V_G = 0$. For $U = 15$ we find a region of negative differential conductance in the region $|V_B| = |J| < 0.5$ (c.f. Fig. 12).

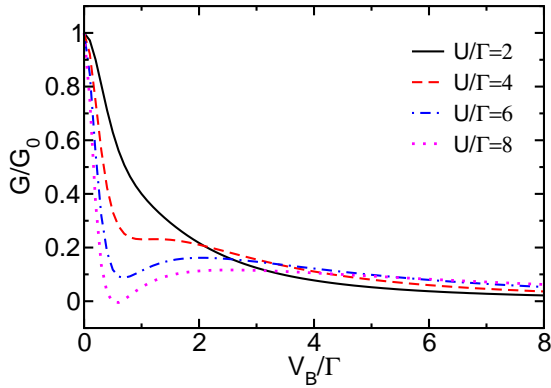


FIG. 12: (color online) Differential conductance G as function of V_B for $V_G = 0$ and various values of U . For $U = > 5$ a distinct minimum around $V_B = 0.5$ appears.

whether the negative differential conductance we find for still larger values of U (c.f. Fig. 12) is a true feature of the model or rather an artifact of the approximations used is presently not clear and should be clarified in further investigations. However, negative differential conductance has also been observed in a slave-boson treatment of the model.⁶³

Keeping $V_G = 0$ fixed, we can calculate the conductance $G = dJ/dV_B$ as function of V_B for different values of U . The results are collected in Fig. 12. In contrast to the simple approximation without flow of the vertex, the conductance is now strongly dependent on U , except for $V_B = 0$, where due to the unitary limit at $T = 0$ we always find $G = G_0$. As already anticipated from the current in Fig. 11, a minimum in G starts to form around $V_B = 0.5$ for $U = > 5$, which is accompanied by a peak at $V_B = 2$. A similar behavior in the conductance was observed in a perturbative treatment,⁵⁶ which in contrast to our current approximation involves the full

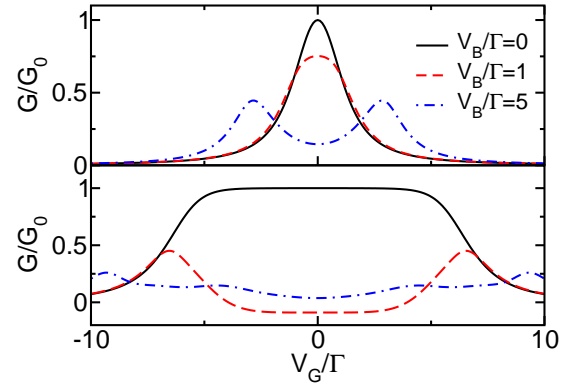


FIG. 13: (color online) Differential conductance G as function of V_G for different values of V_B and $U = 1$ (upper panel) and $U = 15$ (lower panel). Note the extended plateau at $V_B = 0$ for $U = 15$, which is a manifestation of the pinning of spectral weight at the Fermi level.

energy-dependence in the self-energy. This at least qualitative agreement (we of course cannot resolve structures like the Hubbard bands with an energy independent self-energy) again supports our claim that despite the violation of the relation (46) we can obtain reasonable results from G .

We finally discuss the variation of the conductance with V_G for fixed U and V_B . We again emphasize, that for $V_G \neq 0$, $J = 0$ only holds to leading order in U . In Fig. 13 we present the curves for two different values of U , namely $U = 1$ (upper panel in Fig. 13) and $U = 15$ (lower panel in Fig. 13). In the former case, the variation of G with V_B is rather smooth, as is to be expected from the current in Fig. 11. For large U , we observe an extended plateau at zero bias, which is a manifestation of the fact that in the strong coupling regime a pinning of spectral weight at the Fermi energy occurs. This feature is also observed in the imaginary-time RG as well as in NRG calculations.³⁹ Increasing V_B quickly leads to a similarly extended region of negative differential conductance, which, assuming that this result is a true feature of the model, therefore seems to be linked to the "Kondo" pinning. We note that it is unlikely that the appearance of the negative differential conductance is related to the breaking of current conservation at order U^2 as it also appears for $V_G = 0$ where $J = 0$. For large V_B multiple structures appear in G , which are related to the energy scales V_B and U .

IV. SUMMARY AND OUTLOOK

Starting from a generating functional proposed by Kamenev⁴³ we have derived an infinite hierarchy of differential equations for the vertex functions of an interacting quantum mechanical many-body system in nonequilibrium (see also Refs. 25 and 26). The major difference

to the imaginary-time formulation comes from the use of Keldysh Green functions. The indices $+$ and $-$ referring to the upper and lower branch of the (real)-time contour lead to an additional matrix structure to the problem. Our formulation is sufficiently general that it allows to treat bosonic and fermionic models with or without explicit time dependence and at $T = 0$. Since the fRG leads to an infinite hierarchy of coupled differential equations, one has to introduce approximations, at least a truncation at a certain level. Typically one neglects the flow of the three-particle vertex. As has been demonstrated in Ref. 24 for the imaginary-time fRG one can solve the remaining system of flow equations for simple models like the SIAM numerically, thus keeping the full energy-dependence. Due to the fact that the vertex function carries three continuous frequency arguments in addition to the discrete quantum numbers of the system, such a calculation can become computationally quite expensive.

To reduce the numerical effort, further additional approximations can be introduced. A particularly important and successful one is obtained by neglecting the energy dependence of the vertex functions,^{38,39} which already leads to a surprisingly accurate description of local and transport properties of interacting quantum dots in the linear response regime.

We applied the nonequilibrium fRG to the SIAM with finite bias voltage in the stationary state. It turned out,

that for the simplest approximation where only the flow of the self-energy is kept, the analytic structure of the differential equation leads to problems in the numerical solution. In addition, this approximation leads to a violation of the causality relation (46) to order U^2 . The first problem was resolved by including the two-particle vertex in the flow at least up to the largest interaction considered here ($U = 15$). At the present stage this was for computational reasons done by assuming it to be energy-independent, yielding again an energy-independent self-energy. Although this approximation also violates Eq. (46) to order U^2 for a fixed V_G and V_B the error is significantly smaller compared to the simplest scheme. We were able to obtain reasonable expressions and numerical results for the current and the conductance using the functions $G^A(\omega)$ instead of $G^R(\omega)$ in the current formula. We reproduced nonequilibrium features of the current and differential conductance known from the application of other approximate methods to the SIAM.

In the more advanced truncation scheme and for $V_G \neq 0$, the current conservation $J = 0$ only holds to leading order in U . This defect can be traced back to the energy independence of the two-particle vertex, leading to finite, but energy-independent χ^+ and χ^- . By a close inspection of formula (36), however, one can see that this deficiency can for example be cured by assuming a coarse-grained energy dependence of the form

$$\omega < -\frac{V_B}{2} : F(\omega) = 2 \Rightarrow \chi^+ = 0, \chi^- = \text{const.} \quad (54)$$

$$-\frac{V_B}{2} < \omega < \frac{V_B}{2} : F(\omega) = 1 \Rightarrow \chi^+ = \chi^- = \text{const.} \quad (55)$$

$$\omega > \frac{V_B}{2} : F(\omega) = 0 \Rightarrow \chi^+ = 0, \chi^- = \text{const.} \quad (56)$$

and corresponding energy dependencies for χ^+ and χ^- . Here the const. might depend on ω but not on ω . Such an approximation will quite likely also reestablish causality Eq. (46). Work along this line is in progress.

Including finite temperature, magnetic field etc. in the calculations of transport is easily possible, as well as the extension to more complicated "impurity" structures (see e.g. Ref. 39). The latter aspect is typically a rather cumbersome step for other methods like perturbation theories or in particular numerical techniques.

Our present stage of work should mainly be seen as a "proof of principle". Already for the SIAM there remain a variety of fundamental things to do; like the implementation of the full energy-dependence in the calculations, which then should cure the violation of charge conservation and causality; or implementing a reasonable "cut-

off scheme" for time-dependent problems so equilibrium, e.g. to calculate current transients. Despite its current limitations we expect the real-time nonequilibrium formulation of the fRG to be a useful tool to understand nonequilibrium features of mesoscopic systems, just like the imaginary-time version in the calculation of equilibrium properties.

Acknowledgments

We acknowledge useful conversations with H. Schoeller, S. Jakobs, S. Kehrein, J. Koha, H. Monien, A. Schiller, A. Dirks, J. Freericks, K. Ueda, T. Fujii, K. Thygesen, and F. B. Anders. We thank H. Schmidt for pointing out typos in an earlier version of our paper.

This work was supported by the DFG through the collaborative research center SFB 602. Computer support was provided through the Gesellschaft für wissenschaftliche

Datenverarbeitung in Göttingen and the Norddeutsche Verbund für Hoch- und Hochleistungsrechnen.

APPENDIX A: DERIVATION OF THE FLOW EQUATIONS

Although the following derivation is mainly equivalent to the one presented in Ref. 24, the appearance of the factor i in the real-time formulation of the generating functional leads to some changes in signs and prefactors in the equations. It thus appears to be helpful for the reader to repeat the derivation.

As a first step we differentiate W^{ci} with respect to \hat{Q} , which after straightforward algebra leads to

$$\frac{d}{d\hat{Q}} W^{ci} = \text{Tr} \hat{Q} \hat{G}^{0i} + i \text{Tr} \hat{Q} \frac{2W^{ci}}{\hat{Q}} + \frac{W^{ci}}{\hat{Q}} \hat{Q} \frac{W^{ci}}{\hat{Q}} : \quad (\text{A } 1)$$

Considering \hat{Q} and \hat{G} as the fundamental variables we obtain from Eq. (16)

$$\frac{d}{d\hat{Q}} f(\hat{G}; \hat{Q}) = \frac{d}{d\hat{Q}} W^{ci} f(\hat{G}; \hat{Q}) + \frac{d}{d\hat{Q}} \hat{G} : \quad (\text{A } 2)$$

Applying the chain rule and using Eq. (A 1) this leads to

$$\frac{d}{d\hat{Q}} = \text{Tr} \hat{Q} \hat{G}^{0i} + i \text{Tr} \hat{Q} \frac{2W^{ci}}{\hat{Q}} ;$$

where the last term in Eq. (16) cancels a corresponding contribution arising in (A 1) thus a posteriori justifying the inclusion of this term.

Extending the well known relation⁴⁴ between the second functional derivatives of \hat{G} and W^c to nonequilibrium we obtain the functional differential equation

$$\frac{d}{d\hat{Q}} = \text{Tr} \hat{Q} \hat{G}^{0i} + \text{Tr} \hat{Q} V^{1i1} (; \hat{G}^{0i}) ; \quad (\text{A } 2)$$

where V^{1i1} stands for the upper left block of the matrix

$$V ; (; \hat{G}^{0i}) = \begin{pmatrix} 0 & h \\ i \frac{2}{\hat{Q}} & \hat{G}^{0i} \end{pmatrix} \begin{pmatrix} i \frac{2}{\hat{Q}} & h \\ i \frac{2}{\hat{Q}} + \hat{G}^{0i} & i \frac{1}{\hat{Q}} \end{pmatrix} \begin{pmatrix} 1 \\ C \\ A \end{pmatrix} \quad (\text{A } 3)$$

and the upper index t denotes the transposed matrix. To obtain differential equations for the \hat{G}_m which include self-energy corrections we express $V ;$ in terms of \hat{G} instead of \hat{G}^{0i} . This is achieved by defining

$$U ; = i \frac{2}{\hat{Q}} - \hat{G}^{0i}$$

and using

$$\hat{G} = \hat{G}^{0i} + U ; \hat{G}^{0i} ; \quad (\text{A } 4)$$

which leads to

$$\frac{d}{d\hat{Q}} = \text{Tr} \hat{Q} \hat{G}^{0i} + \text{Tr} \hat{G} \hat{Q} V^{1i1} (; \hat{G}) ; \quad (\text{A } 5)$$

with

$$V ; ; \hat{G} = \begin{pmatrix} 0 & h \\ i \frac{2}{\hat{Q}} & \hat{G}^{0i} \end{pmatrix} \begin{pmatrix} h \\ i \frac{2}{\hat{Q}} + \hat{G}^{0i} \end{pmatrix} \begin{pmatrix} 1 \\ C \\ A \end{pmatrix} = \begin{pmatrix} 0 & h \\ i \frac{2}{\hat{Q}} & \hat{G}^{0i} \end{pmatrix} \begin{pmatrix} h \\ i \frac{2}{\hat{Q}} + \hat{G}^{0i} \end{pmatrix} \begin{pmatrix} 1 \\ C \\ A \end{pmatrix} : \quad (\text{A } 6)$$

It is important to note that U_i , as well as $\frac{\partial^2}{\partial \phi_i^2}$ and $\frac{\partial^2}{\partial \phi_j^2}$ are at least quadratic in the external sources. The initial condition for the exact functional differential equation (A5) can either be obtained by lengthy but straightforward algebra, which we are not going to present here or by the following simple argument: at $\phi = 0$, $\hat{G}^{(0)} = 0$ (no degrees of freedom are "turned on") and in a perturbative expansion of the $\Gamma_m^{(0)}$ the only term which does not vanish is the bare two-particle vertex. We thus find

$$\Gamma_m^{(0)}(f, g; f, g) = S_{\text{int}}(f, g; f, g) : \quad (\text{A } 7)$$

Expanding Γ_i , Eq. (A6) in a geometric series

$$\Gamma_i = 1 + \hat{G} U_i + \hat{G} U_i \hat{G} U_i + \hat{G} U_i \hat{G} U_i \hat{G} U_i + \dots + \hat{G}^{i+1} U_i^i + \dots \quad (\text{A } 8)$$

and Γ_m in a Taylor series with respect to the external sources

$$\Gamma_m(f, g; f, g) = \sum_{n=0}^{\infty} \frac{(i)^n}{(n!)^2} \sum_{\substack{X \\ m=0}}^{\infty} \sum_{\substack{X \\ m=0}}^{\infty} \Gamma_m^{(0)} \left(\begin{smallmatrix} 0 \\ 1 \end{smallmatrix}; \dots; \begin{smallmatrix} 0 \\ m \end{smallmatrix}; \begin{smallmatrix} 0 \\ 1 \end{smallmatrix}; \dots; \begin{smallmatrix} 0 \\ m \end{smallmatrix} \right) \begin{smallmatrix} 0 \\ 1 \end{smallmatrix} \dots \begin{smallmatrix} 0 \\ m \end{smallmatrix} \begin{smallmatrix} 0 \\ 1 \end{smallmatrix} \dots \begin{smallmatrix} 0 \\ m \end{smallmatrix} : \quad (\text{A } 9)$$

one can derive an exact infinite hierarchy of flow equations for the Γ_m . For example, the flow equation for the single-particle vertex Γ_1 (the self-energy) can be obtained by taking the expansion (A8) up to first order in U_i , inserting it into (A5), replacing Γ_m on both sides by the expansion (A9) and comparing the terms quadratic in the external fields. This procedure leads to the expression (20).

APPENDIX B: FLOW EQUATION FOR THE TWO-PARTICLE VERTEX

To obtain the flow equation for $\hat{\Gamma}_2$ we have expanded Eq. (A6) in a geometric series up to first order and (A9) in the external sources up to $m = 2$. To find the flow equation for the vertex function, Γ_2 , we have to proceed one step further, that is expand (A6) up to the second order and (A9) up to $m = 3$. After comparison of the terms with the same power in the fields we obtain an expression similar to the equilibrium one (see Eq. (15) of Ref. 39)

$$\begin{aligned} \frac{d}{d\lambda} \Gamma_2 \left(\begin{smallmatrix} 0 \\ 1 \end{smallmatrix}; \begin{smallmatrix} 0 \\ 2 \end{smallmatrix}; \begin{smallmatrix} 0 \\ 1 \end{smallmatrix}; \begin{smallmatrix} 0 \\ 2 \end{smallmatrix} \right) = & \sum_{\substack{X \\ 3; 3}}^{\infty} \sum_{\substack{X \\ 4; 4}}^{\infty} \sum_{\substack{X \\ i; i}}^{\infty} G_{\substack{0 \\ 3}; \substack{0 \\ 3}} S_{\substack{4; 4}}^{\substack{0 \\ 4}} \Gamma_2 \left(\begin{smallmatrix} 0 \\ 1 \end{smallmatrix}; \begin{smallmatrix} 0 \\ 2 \end{smallmatrix}; \begin{smallmatrix} 0 \\ 3 \end{smallmatrix}; \begin{smallmatrix} 0 \\ 4 \end{smallmatrix} \right) + \Gamma_2 \left(\begin{smallmatrix} 0 \\ 3 \end{smallmatrix}; \begin{smallmatrix} 0 \\ 4 \end{smallmatrix}; \begin{smallmatrix} 0 \\ 1 \end{smallmatrix}; \begin{smallmatrix} 0 \\ 2 \end{smallmatrix} \right) \\ & + G_{\substack{3; 3}}^{\substack{0 \\ 3}} S_{\substack{4; 4}}^{\substack{0 \\ 4}} \Gamma_2 \left(\begin{smallmatrix} 0 \\ 1 \end{smallmatrix}; \begin{smallmatrix} 0 \\ 4 \end{smallmatrix}; \begin{smallmatrix} 0 \\ 1 \end{smallmatrix}; \begin{smallmatrix} 0 \\ 3 \end{smallmatrix} \right) + \Gamma_2 \left(\begin{smallmatrix} 0 \\ 3 \end{smallmatrix}; \begin{smallmatrix} 0 \\ 2 \end{smallmatrix}; \begin{smallmatrix} 0 \\ 4 \end{smallmatrix}; \begin{smallmatrix} 0 \\ 2 \end{smallmatrix} \right) \\ & + \Gamma_2 \left(\begin{smallmatrix} 0 \\ 1 \end{smallmatrix}; \begin{smallmatrix} 0 \\ 3 \end{smallmatrix}; \begin{smallmatrix} 0 \\ 1 \end{smallmatrix}; \begin{smallmatrix} 0 \\ 4 \end{smallmatrix} \right) + \Gamma_2 \left(\begin{smallmatrix} 0 \\ 4 \end{smallmatrix}; \begin{smallmatrix} 0 \\ 2 \end{smallmatrix}; \begin{smallmatrix} 0 \\ 3 \end{smallmatrix}; \begin{smallmatrix} 0 \\ 2 \end{smallmatrix} \right) \\ & + \Gamma_2 \left(\begin{smallmatrix} 0 \\ 2 \end{smallmatrix}; \begin{smallmatrix} 0 \\ 4 \end{smallmatrix}; \begin{smallmatrix} 0 \\ 1 \end{smallmatrix}; \begin{smallmatrix} 0 \\ 3 \end{smallmatrix} \right) + \Gamma_2 \left(\begin{smallmatrix} 0 \\ 3 \end{smallmatrix}; \begin{smallmatrix} 0 \\ 1 \end{smallmatrix}; \begin{smallmatrix} 0 \\ 4 \end{smallmatrix}; \begin{smallmatrix} 0 \\ 2 \end{smallmatrix} \right) \\ & + \Gamma_2 \left(\begin{smallmatrix} 0 \\ 2 \end{smallmatrix}; \begin{smallmatrix} 0 \\ 3 \end{smallmatrix}; \begin{smallmatrix} 0 \\ 1 \end{smallmatrix}; \begin{smallmatrix} 0 \\ 4 \end{smallmatrix} \right) + \Gamma_2 \left(\begin{smallmatrix} 0 \\ 4 \end{smallmatrix}; \begin{smallmatrix} 0 \\ 1 \end{smallmatrix}; \begin{smallmatrix} 0 \\ 3 \end{smallmatrix}; \begin{smallmatrix} 0 \\ 2 \end{smallmatrix} \right) ; \quad (\text{B } 1) \end{aligned}$$

where the contribution involving Γ_3 was replaced by its initial value, i.e. $\Gamma_3 = \Gamma_3^{(0)} = 0$. The main difference to equilibrium is the presence of mixed contractions for the Keldysh indices of the matrices \hat{G} and \hat{S} and the four-index tensors Γ_2 .

Up to this point the derivation of the flow equation for the two-particle vertex was as general as the discussion in Sec. II. We now consider the application to the steady state current through a quantum dot described by the SIAM presented in Sec. III. We thus go over to frequency space and introduce the cutoff as in Eq. (40). The single-particle quantum number in Γ is given by the spin index. We can take advantage of spin and energy conservation which implies that the lower indices of \hat{G}

and \hat{S} are equal, that is $\Gamma_3 = \Gamma_3^{(0)}$ and $\Gamma_4 = \Gamma_4^{(0)}$. This does not hold for the Keldysh indices. The integrals over $\Gamma_3^{(0)}$ and $\Gamma_4^{(0)}$ as well as the sums over $\Gamma_3^{(0)}$ and $\Gamma_4^{(0)}$ can then be performed trivially. Using the Morris lemma,²¹ we can rewrite the matrix product of \hat{G} and \hat{S} as

$$\hat{G}(\omega) \hat{S}(\omega) = \frac{1}{2} (\Gamma_3^{(0)} \Gamma_4^{(0)}) \hat{G}_d(\omega) \hat{G}_d(\omega) ;$$

with

$$\hat{G}_d(\omega) = \frac{1}{\Gamma_{d;0}(\omega) + \frac{1}{\Gamma_d(\omega)}} ;$$

The Γ -function can be used to perform another of the

frequency integrals, and the remaining one can be evaluated because of energy conservation of the two-particle

vertex. Using the spin independence of the Green function for zero magnetic field, this leads to

$$\begin{aligned} \frac{d}{d} \begin{matrix} 0; 0; 1; 2 \\ 1; 2; 1; 2 \end{matrix} &= \frac{1}{4} \sum_{\substack{3; 4 \\ i; i}} \begin{matrix} X & X & X \\ G_d^{i^*}(\omega) & G_d^{i^*}(\omega) & G_d^{i^*}(\omega) \end{matrix} \begin{matrix} 0; 0; 3; 4 \\ 1; 2; 3; 4 \end{matrix} \begin{matrix} i \\ i \end{matrix} \\ &+ \sum_{\substack{3; 4 \\ i; i}} \begin{matrix} X & X & X \\ G_d^{i^*}(\omega) & G_d^{i^*}(\omega) & G_d^{i^*}(\omega) \end{matrix} \begin{matrix} 0; 0; 1; 2 \\ 1; 2; 3; 4 \end{matrix} \begin{matrix} i \\ i \end{matrix} \\ &+ \sum_{\substack{3; 4 \\ i; i}} \begin{matrix} X & X & X \\ G_d^{i^*}(\omega) & G_d^{i^*}(\omega) & G_d^{i^*}(\omega) \end{matrix} \begin{matrix} 0; 0; 3; 4 \\ 1; 2; 3; 4 \end{matrix} \begin{matrix} i \\ i \end{matrix} \quad (B2) \end{aligned}$$

Comparing (B2) with Eq. (20) in Ref. 39, where similar approximations were made in equilibrium, we see that we have two more terms because of the Keldysh indices. In the first term appears $G_d^{i^*}$, while its transpose $G_d^{i^*}$ enters everywhere else.

Using the antisymmetry of χ_2 in the spin indices and spin conservation we can further simplify Eq. (B2) by introducing the flowing interaction U^{i^*} defined as

$$\begin{matrix} 0; 0; 1; 2 \\ 1; 2; 1; 2 \end{matrix} = \begin{matrix} 0; 0; 1; 2 \\ 1; 2; 1; 2 \end{matrix} U^{i^*} + \begin{matrix} 0; 0; 1; 2 \\ 1; 2; 1; 2 \end{matrix} U^{i^*} :$$

This leads to the following equation

$$\begin{aligned} \frac{d}{d} U^{i^*} &= \frac{1}{4} \sum_{\substack{3; 4 \\ i; i}} \begin{matrix} X & X \\ G_d^{i^*}(\omega) & G_d^{i^*}(\omega) \end{matrix} U^{i^*} U^{i^*} + U^{i^*} U^{i^*} \\ &+ \sum_{\substack{3; 4 \\ i; i}} \begin{matrix} X & X \\ G_d^{i^*}(\omega) & G_d^{i^*}(\omega) \end{matrix} 2U^{i^*} U^{i^*} + U^{i^*} U^{i^*} \\ &+ \sum_{\substack{3; 4 \\ i; i}} \begin{matrix} X & X \\ G_d^{i^*}(\omega) & G_d^{i^*}(\omega) \end{matrix} U^{i^*} U^{i^*} : \quad (B3) \end{aligned}$$

From the initial value of χ_2 at $\omega = 0$ given in Eq. (38) we can read off as the initial value for U^{i^*}

while all other components are zero.

$$U^{i^*} = iU ;$$

-
- ¹ L.P. Keldysh, JETP 20, 1018 (1965).
² A. Fetter and J. Walecka, Quantum Theory of Many-Particle Systems, International Series in Pure and Applied Physics (McGraw-Hill, New York, 1971).
³ U. Schollwöck, Rev. Mod. Phys. 77, 259 (2005).
⁴ T. Costi, Phys. Rev. B 55, 3003 (1997).
⁵ F.B. Anders and A. Schiller (2006), cond-mat/0604517.
⁶ D. Lobaskin and S. Kehrein, Phys. Rev. B 71, 193303 (2005).
⁷ Y. Meir and N.S. Wingreen, Phys. Rev. Lett. 68, 2512 (1992).
⁸ V. Korenman, Ann. of Phys. 39, 72 (1966).
⁹ D. Langreth, in NATO advanced study institute Series B, edited by J. Devreese and E. van Doren (Plenum New York/London, 1967), vol. 17.
¹⁰ B.A. Itshuler and Y. Aharonov, JETP 48, 812 (1978).
¹¹ K.G. Wilson, Rev. Mod. Phys. 47, 773 (1975).
¹² H. Schoeller, in Low-Dimensional Systems, edited by T. Brandes (Springer Verlag, 1999), vol. 17, p. 137.
¹³ H. Schoeller and J. König, Phys. Rev. Lett. 84, 3686 (2000).
¹⁴ M. Keil and H. Schoeller, Phys. Rev. B 63, 180302 (2001).
¹⁵ A. Rosch, J. Paaske, J. Köhler, and P. Wölfe, Phys. Rev. Lett. 90, 076804 (2003).
¹⁶ A. Rosch, J. Paaske, J. Köhler, and P. Wölfe, J. Phys. Soc. Jpn. 74, 118 (2005).
¹⁷ F. Wegner, Ann. Physik (Leipzig) 3, 77 (1994).
¹⁸ S.D. Glazek and P.B. Wiegmann, Phys. Rev. D 48, 5863 (1993).
¹⁹ J. Polchinski, Nucl. Phys. B 231, 269 (1984).
²⁰ C. Wetterich, Phys. Lett. B 301, 90 (1993).
²¹ T.R. Morris, Int. J. Mod. Phys. A 9, 2411 (1994).
²² M. Salmhofer, Renormalization (Springer, Berlin, 1998).
²³ M. Salmhofer and C. Honerkamp, Prog. Theor. Phys. 105, 1 (2001).
²⁴ R. Hedden, V. Meden, T. P. Ruschke, and K. Schonhammer,

- J. Phys.: Condens. Matter 16, 5279 (2004).
- ²⁵ S. Jakobs, Diploma thesis, RWTH Aachen (2003).
- ²⁶ S. Jakobs, V. Meden, and H. Schoeller, in preparation.
- ²⁷ L. Canet, B. Delamotte, O. Delubriere, and N. Wschebor, Phys. Rev. Lett. 92, 195703 (2004).
- ²⁸ P. W. Anderson, Phys. Rev. 124, 41 (1961).
- ²⁹ M. A. Kastner, Rev. Mod. Phys. 64, 849 (1992).
- ³⁰ L. P. Kouwenhoven, D. G. Austing, and S. Tarucha, Rep. Prog. Phys. 64, 701 (2001).
- ³¹ J. Nygard, D. H. Cobden, and P. E. Lindelof, Nature 408, 342 (2000).
- ³² V. Madhavan, W. Chen, T. Jamneala, M. F. Crommie, and N. S. Wingreen, Science 280, 567 (1998).
- ³³ J. Li, W.-D. Schneider, R. Berndt, and B. Delley, Phys. Rev. Lett. 80, 2893 (1998).
- ³⁴ G. A. Fiete and E. J. Heller, Rev. Mod. Phys. 75, 933 (2003).
- ³⁵ M. Pustilnik and L. Glazman, J. Phys.: Condens. Matter 16, R513 (2004).
- ³⁶ A. Georges, G. Kotliar, W. Krauth, and M. J. Rozenberg, Rev. Mod. Phys. 68, 13 (1996).
- ³⁷ T. Maier, M. Jarrell, T. Pruschke, and M. H. Hettler, Rev. Mod. Phys. 77, 1027 (2005).
- ³⁸ S. Andergassen, T. Enss, and V. Meden, Phys. Rev. B 73, 153308 (2006).
- ³⁹ C. Karrasch, T. Enss, and V. Meden, Phys. Rev. B 73, 235337 (2006).
- ⁴⁰ L. Landau and E. Lifshitz, Physical Kinetics (Akademie-Verlag Berlin, 1983).
- ⁴¹ J. Rammer and H. Smith, Rev. Mod. Phys. 58, 323 (1986).
- ⁴² H. Haug and A.-P. Jauho, Quantum Kinetics and Optics of Semiconductors (Springer Verlag, 1996).
- ⁴³ A. Kamenev, in Les Houches, Volume Session LX, edited by H. Bouchiat, Y. Gefen, S. Geron, G. Montambaux, and J. Dalibard (Elsevier, North-Holland, 2004), cond-mat/0412296.
- ⁴⁴ J. Negele and H. Orland, Quantum Many-Particle Physics (Addison-Wesley, 1988).
- ⁴⁵ C. Honerkamp, D. Rohe, S. Andergassen, and T. Enss, Phys. Rev. B 70, 235115 (2004).
- ⁴⁶ V. Meden, lecture notes on the "Functional renormalization group", <http://www.theorie.physik.uni-goettingen.de/~meden/funRG/>
- ⁴⁷ C. Honerkamp and M. Salmhofer, Phys. Rev. B 67, 174504 (2003).
- ⁴⁸ A. Komnik and A. O. Gogolin, Phys. Rev. Lett. 94, 216601 (2005).
- ⁴⁹ J. E. Han, Phys. Rev. B 73, 125319 (2006).
- ⁵⁰ J. E. Han (2006), cond-mat/0604583.
- ⁵¹ S. Hershfeld, J. H. Davies, and J. W. Wilkins, Phys. Rev. Lett. 67, 3720 (1991).
- ⁵² S. Hershfeld, J. H. Davies, and J. W. Wilkins, Phys. Rev. B 46, 7046 (1992).
- ⁵³ Y. Meir, N. S. Wingreen, and P. A. Lee, Phys. Rev. Lett. 70, 2601 (1993).
- ⁵⁴ A. Levy Yeyati, A. Martn-Rodero, and F. Flores, Phys. Rev. Lett. 71, 2991 (1992).
- ⁵⁵ N. S. Wingreen and Y. Meir, Phys. Rev. B 49, 11040 (1994).
- ⁵⁶ T. Fujii and K. Ueda, Phys. Rev. B 68, 155310 (2003).
- ⁵⁷ J. H. Han (2004), cond-mat/0405477.
- ⁵⁸ M. Hamasaki (2005), cond-mat/0506752.
- ⁵⁹ S. Datta (2006), cond-mat/0603034.
- ⁶⁰ K. Thygesen and A. Rubio (2006), cond-mat/0609223.
- ⁶¹ A. C. Hewson, The Kondo Problem to Heavy Fermions, Cambridge Studies in Magnetism (Cambridge University Press, Cambridge, 1993).
- ⁶² L. P. Kouwenhoven et al., in Mesoscopic Electron Transport, edited by L. L. Sohn et al. (Dordrecht: Kluwer, 1997), p. 105.
- ⁶³ J. Takahashi and S. Tasaki (2006), cond-mat/0603337.